HIGH IMPEDANCE FAULT ARCING ON SANDY SOIL IN 15kV DISTRIBUTION FEEDERS: CONTRIBUTIONS TO THE EVALUATION OF THE LOW FREQUENCY SPECTRUM

A. E. Emanuel, Senior Member, IEEE
D. Cyganski, J. A. Orr, Members, IEEE
S. Shiller
Worcester Polytechnic Institute
Worcester, MA 01609

E. M. Gulachenski
Senior Member, IEEE

New England Power Service Co.
Westborough, MA 01581

ABSTRACT

This paper presents the measured values of current harmonics at a staged high impedance ground fault on sandy soil. The measured low frequency spectrum is compared with current harmonics recorded continuosly for one week at the substation. This comparison was carried out to determine to what extent 120 Hz and 180 Hz components may be used to help detect a high impedance fault. The field measurements are supported by a simple theoretical model and laboratory measurements. It is concluded that for the studied feeder detection of high impedance arcing faults may be possible by monitoring of the second harmonic current.

KEY WORDS: System Protection, Arcing, Harmonics

INTRODUCTION

Engineering efforts for the development of a reliable method for the detection of high impedance ground faults (HIGF) led during the last decade to important progress in understanding the "signature" of the fault current and in the evaluation of several detection concepts [1]. Among many techniques proposed by different research groups [2-6], use of the information contained in the low frequency spectral behavior, in terms of both magnitude and phase, seems to be the most promising approach for the next steps which will bring the industry closer to the realization of a fully operational HIGF detector.

The primary purpose of this paper is to report the fault current spectrum of staged faults on a 13.8kV distribution feeder and to compare the measured components with the neutral current spectrum measured at the substation. The results are evaluated in the context of development of a method for reliable detection of arcing faults without excessive false tripping on non-fault conditions. An elementary theoretical model for arcing on sandy soil is also presented.

89 SM 784-0 PWRD A paper recommended and approved by the IEEE Transmission and Distribution Committee of the IEEE Power Engineering Society for presentation at the IEEE/PES 1989 Summer Meeting, Long Beach, California, July 9 - 14, 1989. Manuscript submitted January 31, 1989; made available for printing May 19, 1989.

STAGED HIGH IMPEDANCE GROUND FAULT FIELD TESTS

The field test was implemented on the system shown in Fig. 1. The feeder is supplied by two three-phase transformers, 69/13.8kV, grounded wye, 7.5 MVA, 7.6% short circuit impedance connected in parallel. At the end of the feeder branch which supplies primarily residential customers, 20,000 ft from the substation, a HIGF was staged by connecting an insulated conductor, via a 10A fuse, to the primary conductor, phase B, of the feeder. The insulated conductor was connected to a 2.5 ft diameter loop of uninsulated copper wire, #2 AWG . By locating the loop nearer to or further from a driven ground rod it was possible to obtain larger or smaller fault currents.

The instrumentation used to monitor the fault current spectrum is described in the Appendix and in reference [7]. Several tests were conducted with different spacings between the energized conductor and the ground rod. Recordings of the fundamental, second and third harmonic currents vs. time are presented in Fig. 2 for a test with relatively large arc current (approximately 15A). Also presented in this figure are the phase angles of the second and third current and voltage harmonics for the same test. A summary of the measurements for a range of test conditions is given in Table I.

It was observed and later confirmed in the laboratory that faults with currents above 1A have a stable arc with nearly constant rms value for long periods of time. Arc currents lower than 1A are characterized by shorter periods of stable arc current, and by random initiation and quenching of the arc. The phase angles of the second and third harmonic currents measured for arcs of 12A and 15A remain within a certain range ($\pm 25^\circ$ for the second and $115^\circ \pm 15^\circ$ for the third harmonic). At lower current the phase angles vary over three quadrants. For currents above 10A, the third harmonic current is between 5%

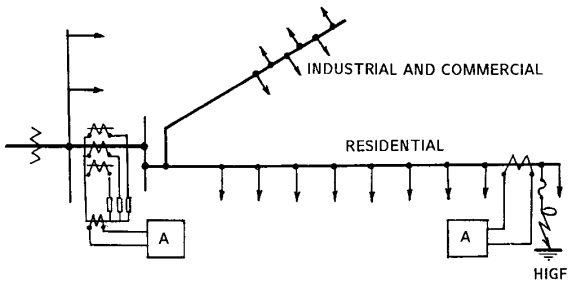

Fig. 1 Diagram of feeder with staged high impedance arcing fault.

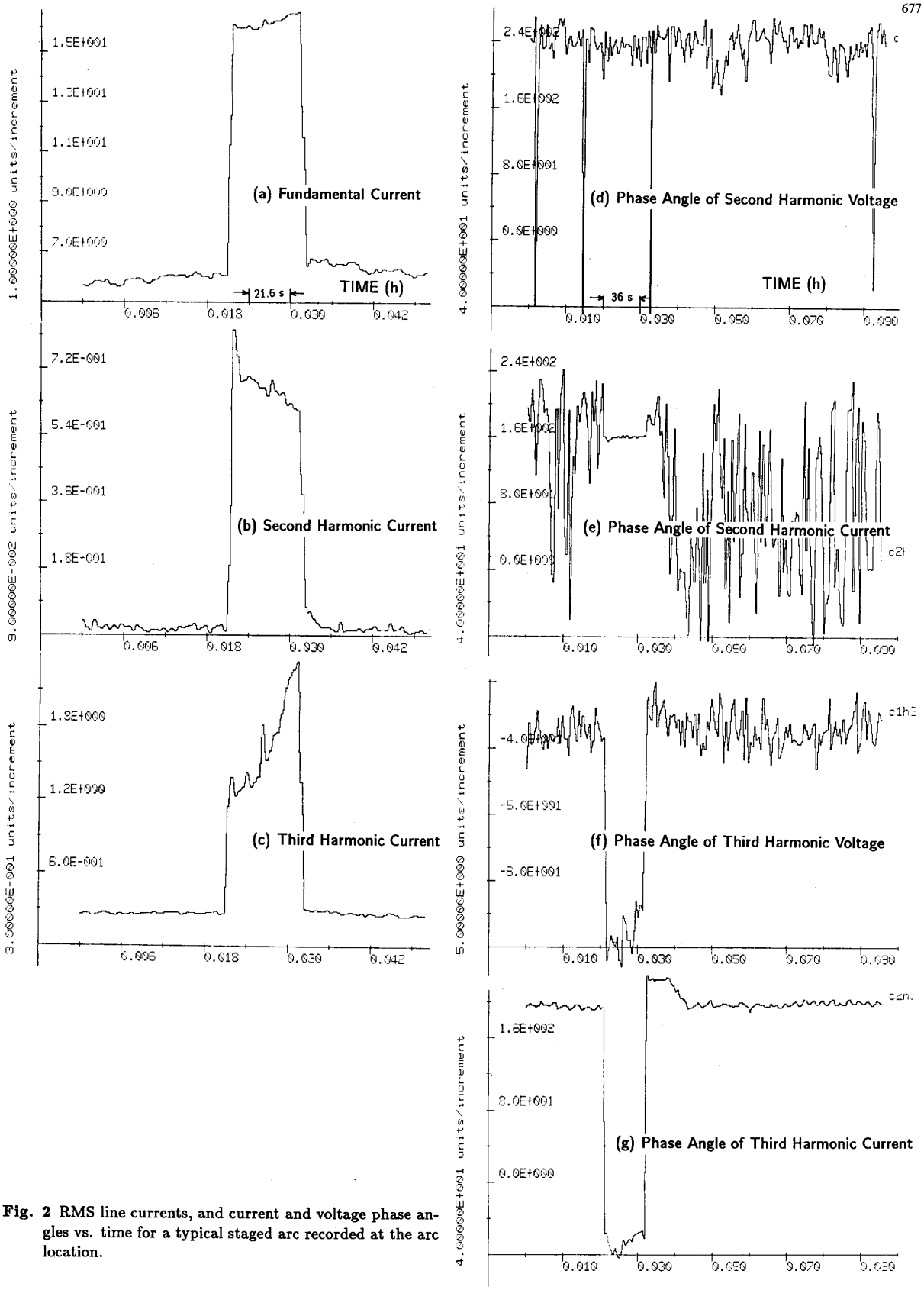

Fig. 2 RMS line currents, and current and voltage phase angles vs. time for a typical staged arc recorded at the arc location.

TABLE I

STAGED HIGF FIELD TESTS MEASUREMENTS SUMMARY

Harmonic Number	Arc Currents: rms Amplitude and phase angle											
	Test # 1				Test # 2				Test # 3			
	(A)		(deg)		(A)		(deg)		(A)		(deg)	
	min	max	min	max	min	max	min	max	min	max	min	max
1	15		-12		12		-10		0	0.9	-10	-8
2	0.56	0.64	-25	25	0.63	0.81	-25	25	0	0.26	-270	80
3	1.2	3.6	100	128	1.2	2.4	102	132	0	0.22	-210	200
4	0.24	0.36	-141	-145	0.24	0.32	-140	-145	undetectable			
5	0.9	1.4			1.2	1.5			0	0.05	120	160
6	0.11	0.17			0.12	0.17			undetectable			
7	0.50	0.80			0.45	0.85			0	0.001	-60	-35
9	0.20	0.50			0.1	0.5			undetectable			
11	0.3	0.55			0.25	0.5			undetectable			
13	0.09	0.36			0.06	0.03			undetectable			

and 15% of the fundamental, and the second harmonic current is between 3.7% and 6.7% of the fundamental. For currents below 1A the 120 Hz component varies from 0% to 3% while the 180 Hz component lies between 0% and 24% of the maximum fundamental value.

Measurements for harmonics above the third are not discussed here because they have not been found to contain reliable, characteristic information for detection of low current arcs.

SUBSTATION CURRENTS

To determine the feasibility of use of an HIGF detector which monitors low frequency harmonics components it is necessary become familiar with the background current harmonics as measured at the substation. Phase and neutral current harmonics were monitored continuously for one week (168 hr). Some graphical results are shown in Fig. 3 for the neutral currents, and results are summarized in Table II. The third harmonic component of the line current is shown in Fig. 4. The minimum, mean, and maximum values are 0.35A, 1.75A, and 3.5A respectively. Comparing the histograms of the third harmonic line current, Fig. 4, with the third harmonic neutral current, Fig. 3f, demonstrates that if the detecting device is based on sensing of the 180 Hz component the sensor should monitor the line (rather than the neutral) current since the background signal is lower on the lines.

The conclusion is opposite for the 120 Hz component where a lower background is found in the neutral current. Table II shows that the minimum, mean, and maximum values of the 120 Hz component are 0A, 0.148A, and 2.7A. The maximum value is usually less than 0.6A; however random bursts reaching as high as 2.7A were observed. The 120 Hz component is governed by the transients in the system. Such transients cause DC biasing of iron core devices and asymmetrical zero voltage crossings which in turn generate 120 Hz components.

The 180 Hz component, which is primarily caused by magnetization currents, has a less random behavior. The relative difference between the maximum and minimum values, Fig. 3e, was found to be significantly smaller than for the differences at 120 Hz (Fig. 3c). The phase angle of the third harmonic was found to be quite stable at 255° ±15°. This value is quite typical for a third harmonic generated by the transformer magnetizing currents.

TABLE II

NEUTRAL CURRENT HARMONICS AT THE SUBSTATION

Harmonic Number	rms current (A)			Std Dev (A)	Phase Angle*
	min	mean	max		
1	17	45	85	34	
2	0	0.148	2.7	0.085	
3	2.9	4.72	6.8	1.03	240° to 270°
4	0.06	0.114	0.32	0.064	
5	0.02	1.394	4.5	1.37	
6	0.05	0.14	0.36	0.08	
7	0.10	0.45	1.4	0.58	
9	0.02	1.65	3.7		
11	0.01	0.20	2.0		
13	0.02	0.18	0.55		

* Phase measured relative to fundamental voltage, phase A

LABORATORY MEASUREMENTS AND THEORETICAL COMPUTATIONS

A simple experiment, Fig. 5, was devised to help display under controlled conditions the behavior of an arc in sandy soil. The secondary voltage (7900V) was applied to a metallic cylindrical container, 30 cm in diameter and 50 cm in height filled with construction grade sand. A variable resistor was connected in series with the container in order to simulate and vary the ground path resistance. The $v - i$ characteristic as well as the current harmonics were measured as functions of the arc current. Following is a brief summary of the principal observations.

The fault current is not symmetrical. The positive half-cycle is larger in amplitude than the negative one. Figure 6 shows oscillograms of currents and voltages which illustrate this property. This characteristic is valid for large as well as for small fault currents, as long as arcing is taking place. This asymmetry is also noticeable in the $v - i$ hysterisis of the arc as well as in the arc voltage which is smaller during the positive half cycle, Fig. 7.

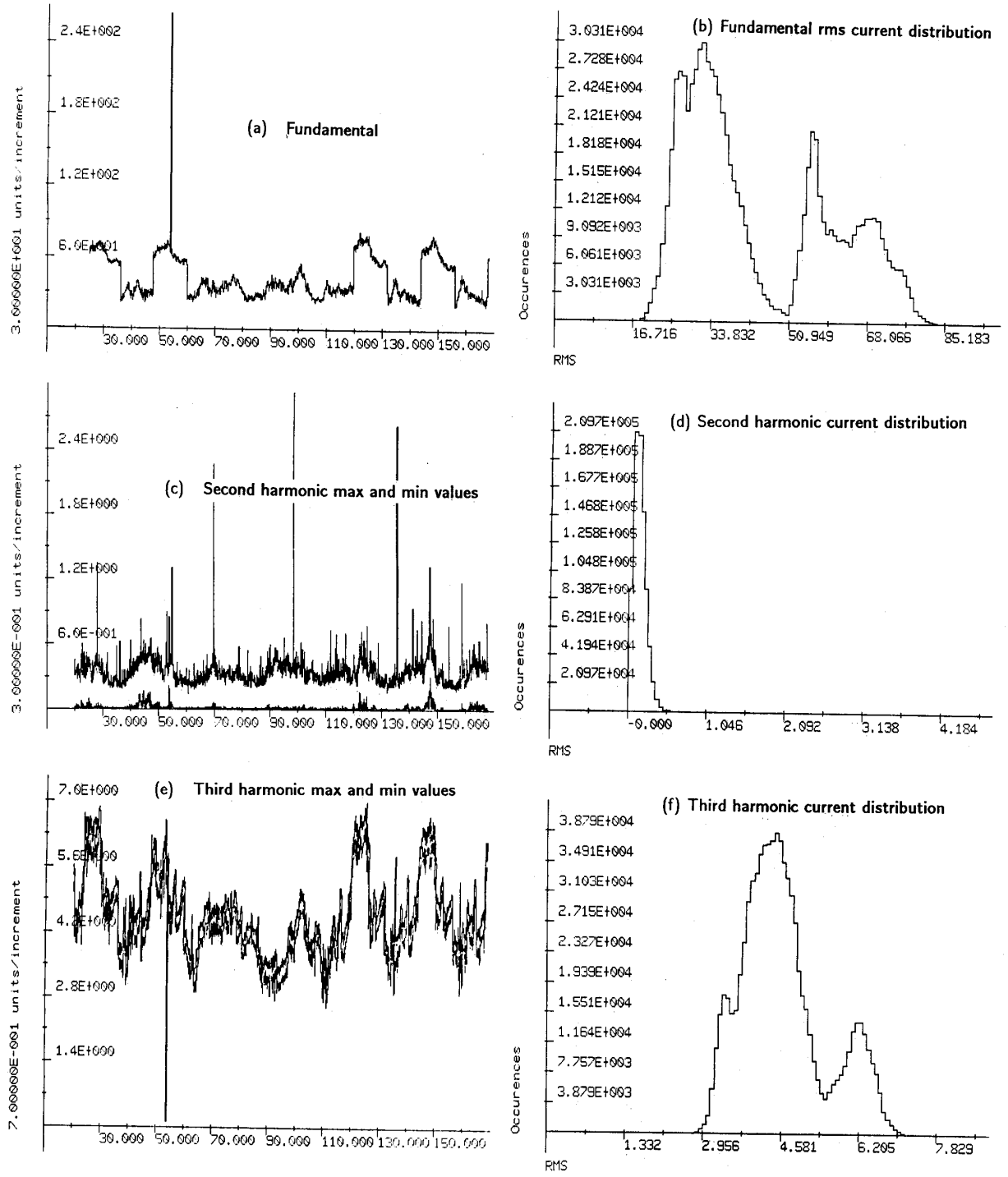

Fig. 3 Weekly recording of neutral currents at the substation.

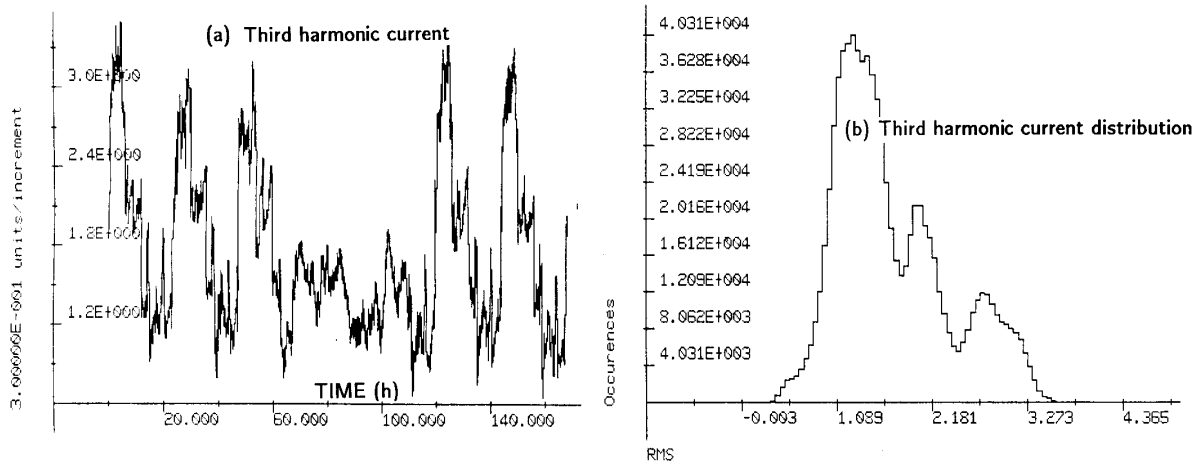

Fig. 4 Third harmonic line currents measured at the substation.

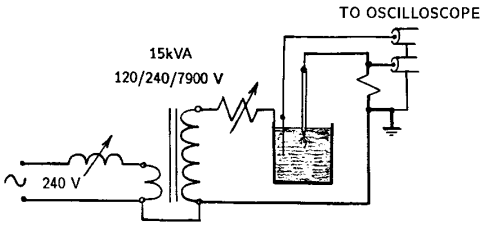

Fig. 5 Schematic of laboratory arc testing arrangement.

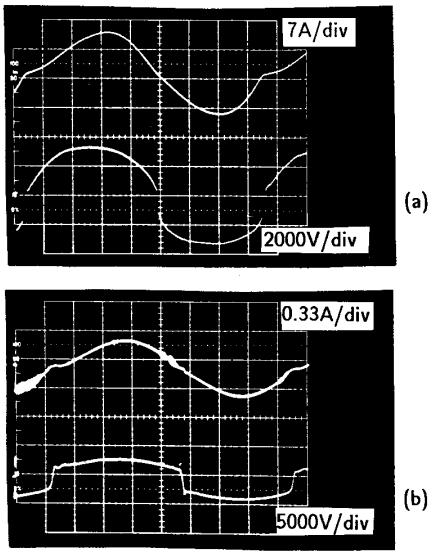

Fig. 6 Oscillograms of laboratory arc currents; (a): large arc current; (b): small arc current.

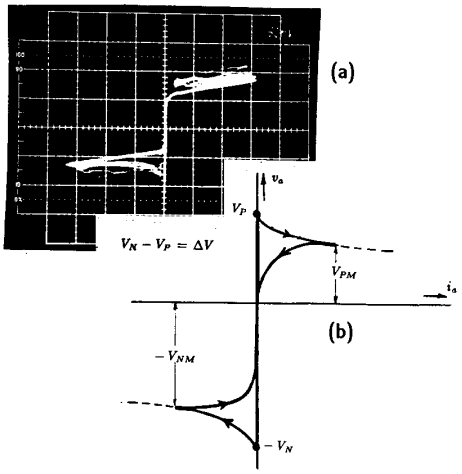

Fig. 7 $v - i$ characteristic of arc; (a): laboratory oscillogram; (b): theoretical description.

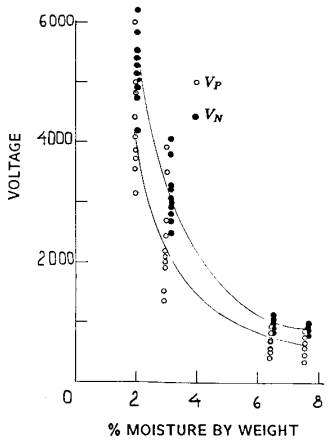

Fig. 8 Arc voltage vs. moisture level of soil.

The onset arc voltages, V_P, V_N (Fig. 7b) are for all practical purposes independent of the high voltage electrode geometry and material (Cu, Al, Fe). The density (porosity) and the amount of moisture of the sandy soil have a major effect on the values of V_P, V_N. Less densely packed soil yields higher onset voltages. Drier soils also cause higher arc voltages. The effect of the soil moisture on the onset arc voltages is shown in Fig. 8. Moisture affects the local geometry of the arcing and the heat transfer conditions. On sandy soil with moisture in excess of 15% to 20% by weight the arc is not triggered immediately. The evolution of the arc on wet soil can be understood with the help of the oscillogram shown in Fig. 9. At the time of energization the current was sinusoidal (no arcing taking place). After a few seconds however, the soil surrounding the electrode heats up; development of steam causes a local increase in porosity and the arc is triggered. In time the arc voltage increases as the arc starts to propagate in the soil.

The development of the arc is presented in Fig. 10. When the arc is triggered, Fig. 10b, the arc tip in the soil will drastically change the distribution of the local electric field, causing a field enhancement at the tip of the arc. Thermionic emission, high field gradients, and the fact that the conductive layer of soil recedes away from the electrode, cause the arc to extend, Fig. 10c, and penetrate into the soil. This type of arc probably owes its pronounced $v-i$ asymmetry to the fact that the glowing hot silica surrounding the arc acts like a "cathodic spot" which emits electrons, causing a smaller voltage drop when the conductor (high voltage electrode) is positive. As the arc extends further into the soil two parameters are changing: (1) the soil surrounding the arcing area becomes dry; (2) the balance between the rate of generation of the heat of arcing and the transferred heat to the environment is disturbed. These result in the arc being quenched, Fig. 10d. From this stage two scenarios are possible:

1. Moisture will diffuse back into the dry soil and the arc will be reignited once the front edge of the moist (conductive) layer is close enough to the high voltage electrode. The arc, however, will be re-triggered on a different path than the previous one. The initial arcing path is now a solidly vitrified form of fulgurites tubes.

2. If the dropped conductor has multiple points of contact with the soil, then another point which was previously inactive may start arcing if the local field has increased due to changes in the potential distribution.

A simple model, Fig. 11, enabled performance of some theoretical calculations. The arc was modeled with the help of two DC sources, V_P, V_N, connected antiparallel by means of two diodes. During the positive half cycle current flows through V_P only. The source $V_N > V_P$, $V_N - V_P = \Delta V$. The second and third harmonic currents (as percent of the fundamental) are presented as functions of ΔV and $\tan\theta = X_L/R$ in Fig. 12a,b. The parameter defining each surface is the voltage V_N. These results are confirmed by the experimental work. The higher the arc voltage becomes, the more distorted is the arc current. While the asymmetry voltage ΔV has a minor effect on the third harmonic current, Fig. 12b, it should be noted that the second harmonic current is generated on account of ΔV only.

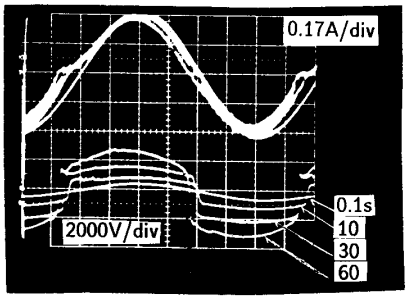

Fig. 9 Oscillogram of arc current and voltage vs. time; upper traces: current; lower traces: voltage.

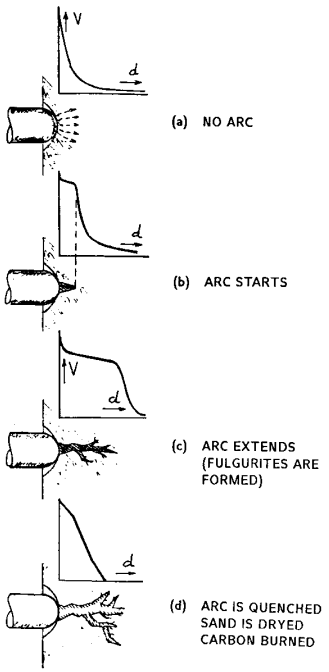

Fig. 10 Physical characteristics of arc environment vs. time.

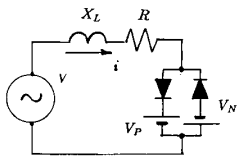

Fig. 11 Circuit model of HIGF with arc.

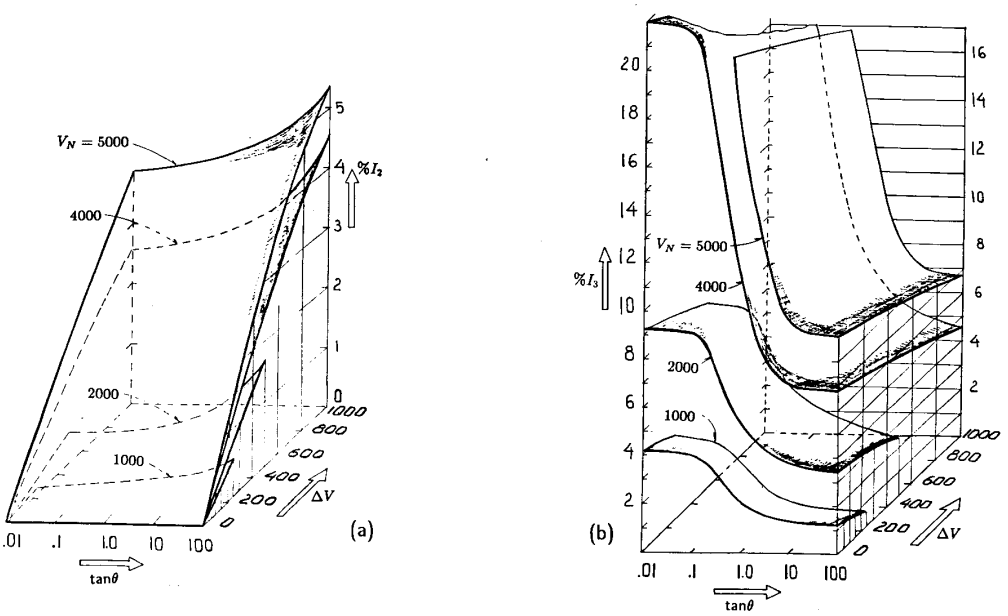

Fig. 12 Arc harmonic current vs. phase angle θ and voltage ΔV; (a): second harmonic current; (b): third harmonic current.

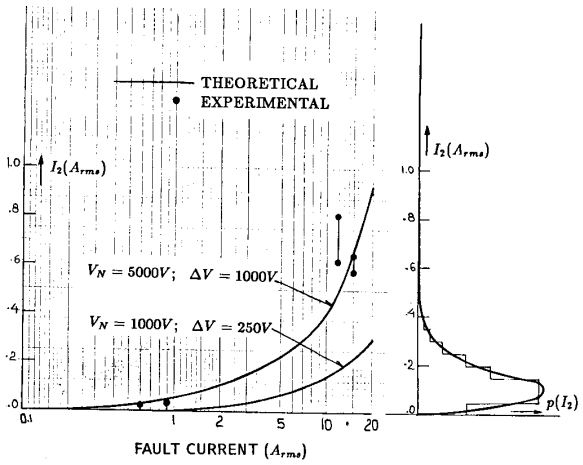

Fig. 13 Comparison of second harmonic arc current to background second harmonic current level. Left graph: second harmonic current vs. total arc current; right graph: measured background distribution of second harmonic current.

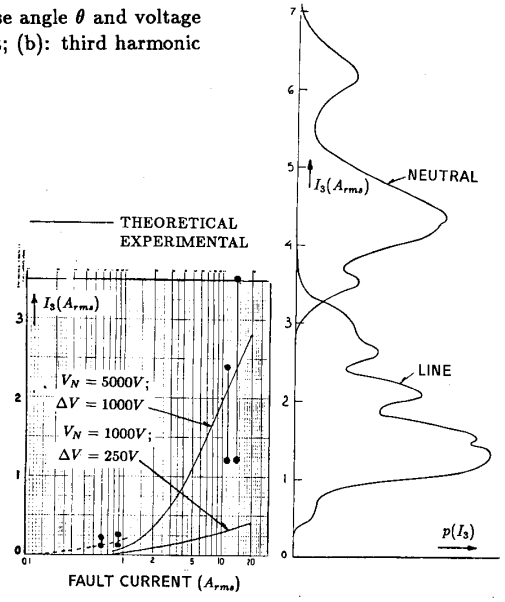

Fig. 14 Comparison of third harmonic arc current to background third harmonic current. Left graph: third harmonic current vs. total arc current; right graph: measured background distribution of third harmonic current for the neutral and the line.

CONCLUSIONS

Figure 13 shows the 120 Hz current versus the fault current. The solid lines represent theoretical values obtained from the elementary model, Fig. 11, assuming $V_N = 5000V$, $\Delta V = 1000V$ (upper line) or $V_N = 1000V$, $\Delta V = 250V$ (lower line). The currents measured during the staged fault are marked with solid dots. On the right side is shown the probability of occurrence of second harmonic current amplitude measured at the substation during normal operation, to enable determination of a threshold for detection of second harmonic current due to arcing. In the same manner the third harmonic arc current vs. fault current is presented in Fig. 14. On the right side the density functions for line and neutral third harmonic currents are shown.

It is confirmed that monitoring of line current rather than neutral current is more appropriate when third harmonic current is used for the purpose of arc detection. Comparing Fig. 13 with Fig. 14 shows that for the particular feeder the use of second harmonic detection would enable identification of lower-amplitude arcs than use of third harmonic currents.

REFERENCES

[1] Aucoin, M., "Status of High Impedance Fault Detection," IEEE Trans PAS, Vol. 104, No. 3, March, 1985, pp. 638-644.

[2] Phadke, A. G., H. E. Hankun, "Detection of Broken Distribution Conductors," Proc. IEEE Southeastern Conf., Raleigh, N. C., CH2161-8/85/0000-0074.

[3] Balser, S. J., K. A. Clements, D. J. Lawrence, "A Microprocessor Based Technique for Detection of High Impedance Faults," IEEE PES Winter Meeting, 1986, Paper No. 86WM152-3.

[4] Graham, H. L., A. J. Carlson, T. A. Granberg, "Broken Conductor and High Impedance Fault Detection by High Frequency Impedance Monitoring," IEEE PES Winter Meeting, 1980, Paper No. A-80-064-6.

[5] Aucoin, B. M., B. D. Russel, "Detection of Distribution High Impedance Faults Using Burst Noise Signals Near 60 Hz," IEEE Trans. on Power Delivery, Vol. 2, No. 2, April, 1987, pp. 342-348.

[6] Russel, B. D., R. P Chincali, C. J. Kim, "Behavior of low Frequency spectra During Arcing Faults and Switching Events," IEEE PES Summer Meeting, San Francisco, CA, 1987, Paper 87SM633-1.

[7] Cyganski, D., J. A. Orr, T. Gentile, "A Time Domain System for Real-time Acquisition and Statistics Calculation for Voltage and Current Waveshapes," Second Intl. Conf. on Harmonics in Power Systems, Winnipeg, Manitoba, Oct. 1986, pp. 270-279.

APPENDIX
HARMONICS MEASUREMENT SYSTEM

The design and operation of a portable, personal computer-based system for the measurement and processing of data on 60 Hz and harmonic current and voltage amplitudes and phases, and for the production of statistics and time trends on those quantities are reviewed in this appendix. More information is contained in reference [7]. The system described here is intended to be more flexible in application than conventional wave and spectrum analyzers, and processes data in real time so that useful results are immediately available in the field. Significant characteristics of this system include the following: extensive use of software rather than hardware to implement signal processing functions; applicability to a wide range of measurements including harmonic and 60 Hz voltage and current, and daily trends; on-line data processing and graphics display eliminating the need for centralized, off-line processing. A relatively low cost system has been achieved by use of commercially-available personal computer equipment and a minimum of custom-build hardware.

Precautions have been taken in the design of this system to avoid sources of error common to digital (as opposed to conventional analog) frequency analysis techniques. These include use of four-pole anti-aliasing filters, a high resolution (12 bit) A/D converter, and phase locked loop to synchronize sampling to the input fundamental frequency (nominally 60 Hz).

Following is a summary of the variables and statistics capable of being measured and calculated during data runs. Additional types of information (such as effects on specific types of equipment) may be derived off-line using these basic results. Over a period of N hours, divided into subintervals of length T seconds, the system calculates and stores for each selected harmonic frequency of each selected voltage or current channel, statistics selected from among: Mean, Mean Square Value, Variance, Maximum, Minimum.

Composite quantities such as real, apparent, and distortive "powers" may also be calculated over the entire interval. The system may also calculate and display phase angle information. The measurement system is almost completely software controlled, and a menu-driven setup algorithm interacts with the operator to establish the measurement conditions for a data run.

The data acquisition hardware and its associated software is designed to have the following characteristics:

1. Eight analog input channels, representing any combination of currents and voltages;
2. Current and voltage magnitude ranges determined by transducers (current and potential transformers);
3. Analog voltage gains of 1 to 100 program selectable to accommodate differing transducer outputs. Full scale transducer output (including effect of current shunt) must lie in the range of 0.1 to 10 volts to achieve desired accuracy.
4. Two frequency ranges with corresponding sampling rates are available: a low frequency range (60 to 1000 Hz) using 1 to 8 channels, and a high frequency range using 1 or 2 channels.
5. On the low frequency range, 32 samples per cycle of the 60 Hz waveforms are taken; on the high frequency range, 128 samples per cycle are taken.

Design factors including the need for portability and moderate cost, together with significant processing capability resulted in the selection of a general-purpose 16 bit IBM PC-compatible computer as the basis for the system.

Only the analog signal conditioning interface and the phase-locked loop system required circuit design and construction. These are described below. Potentially dangerous voltages are isolated by current and potential transformers from the analog and digital electronics. Potential transformers with stepdown ratios of 40:1 are used here. These are appropriate for 120 volt circuits, and may easily be replaced by other PT's for higher voltages. Clamp-on current transformers for the range of 0 to 100 A are used.

A phase lock loop (PLL) circuit is used to synchronize the sampling rate of the A/D converter to the fundamental frequency of the power system being measured. Any deviation from an exact integer multiple relation between sampling rate

and power line frequency results in errors in the calculated harmonic spectrum. These spectrum errors (referred to as the Gibb's phenomenon and the "picket fence effect") can be quite significant even for small deviations in sampling frequency, and are particularly troublesome in attempting to measure low-amplitude harmonics.

Input data is taken during 1/60 sec. time windows, sampled at either 32 or 128 samples per 1/60 sec., and quantized to 4096 levels. The repetition rate of these windows is a function of the amount of statistical processing requested in the particular data run. A typical value is approximately one data window per second.

Software for the system consists of two primary programs, one which assists the user in configuring the system for a data acquisition run and which actually acquires the current and voltage data and performs real-time processing, and another which accesses the stored statistics, formats and displays them in convenient form. At the heart of the data acquisition software is the efficient split radix Fast Fourier Transform algorithm which produces harmonic amplitudes and phase angles from the input time domain data.

BIOGRAPHIES

Alexander E. Emanuel (SM'71) started his engineering training at the Polytechnic Institute of Bucharest, Bucharest, Romania, and graduated from Technion-Israel Institute of Technology, Haifa, Israel.

From 1963 to 1969 he was on the staff of the Electrical Engineering Department at Technion-Israel Institute of Technology, first as a Teaching Assistant and later as Lecturer. From 1969 to 1974 he worked for the High Voltage Power Corporation as Senior Research and Development Engineer. In 1974 he joined Worcester Polytechnic Institute, Worcester, MA. Presently, he holds the rank of Professor, and acts as a consultant to local industry. His expertise is in power electronics, electromechanical energy conversion, and high-voltage technology.

Dr. Emanuel is a Registered Professional Engineer in Massachusetts. He is a member of Sigma Xi, Eta Kappa Nu, Tau Beta Pi, and the Societe Royale Belge des Electriciens. He is the 1982 recipient of the WPI Trustees' Award for Outstanding Teaching, and the 1986 recipient of the WPI Trustees' Award for Outstanding Research.

Edward M. Gulachenski (M'53-SM'66) was born in Hyannis, MA, on October 14, 1930. He received the BS degree in Electrical Engineering from Massachusetts Institute of Technology, Cambridge, MA, and the MS degree in Electrical Engineering from Northeastern University, Boston, MA, in 1952 and 1960, respectively.

He has been employed by New England Electric since 1954, where he was Manager of Electrical System Research from 1973 to 1980. Since 1986 he has held the position of Manager of Relay and Control Engineering.

Edward Gulachenski is a Lecturer in Electrical Engineering at Northeastern University where he teaches Power Circuit Analysis. He has served as Chairman of the EPRI Power System Planning Subcommittee. He is a member of the IEEE Power Engineering Society, has served in the past on the Transformer Committee, and has been associated with the Power System Relay Committee since 1987. He is a registered Professional Engineer in the state of Massachsusetts.

David Cyganski (S'80-M'81) received the PhD degree in Electrical Engineering from Worcester Polytechnic Institute in 1981. From 1977 to 1978 he held the position of Member of Technical Staff at Bell Laboratories, North Andover, MA in the Toll Transmission Division. He is currently Associate Professor of Electrical Engineering at Worcester Polytechnic Institute. His research activities include aspects of image processing, the application of computer technology to power systems analysis, and communications theory.

Dr. Cyganski is a member of Sigma Xi, Eta Kappa Nu, Tau Beta Pi, and Sigma Pi Sigma. He was the first recipient of the Joseph Samuel Satin Distinguished Fellow Award at WPI.

John A. Orr (S'68-M'70-S'74-M'77) received the BS and PhD degrees in Electrical Engineering from the University of Illinois, and the MS degree from Stanford University. He was a Member of Technical Staff at Bell Laboratories, Holmdel, NJ from 1969 to 1974, in the video telephone systems engineering area. He has been at Worcester Polytechnic Institute since 1977, where he currently holds the rank of Professor of Electrical Engineering. His research interests are in the area of digital signal processing, particularly as applied to power systems.

Dr. Orr is a member of Sigma Xi, Eta Kappa Nu, and Tau Beta Pi. He is a recipient of the Joseph Samuel Satin Distinguished Fellow Award in the Electrical Engineering Department at WPI.

Stephen E. Shiller was born in New London, CT, on September 14, 1966. After receiving his B.S. degree in Electrical Engineering from Worcester Polytechnic Institute, Worcester, MA, he begin graduate work, also at WPI. He is currently engaged in an M.S. program. His primary research interest is in communications engineering.

D. I. JEERINGS, J. R. LINDERS, Nordon R. & D.,Inc. Plant City, FL. This paper adds significantly to the understanding of the electrical characteristics of high impedance ground faults (HIGF). We compliment the authors for going directly to the limiting case of very small fault currents. We are pleased to note that not withstanding the different soil conditions, the data in this paper is in agreement with our test data and with the theory which we presented in our paper, "Ground Resistance - Revisited"[1]. The reported variations in phase angle of the 3rd harmonic fault current is within the range we have observed at higher fault currents. The increased magnitude of this harmonic, up to 24%, at these low currents, compared to our measurements of four to 12% at 50 amperes and above, agrees with the above mentioned theory.

The growth of the conducting volume in the soil, as suggested by Fig. 10, should cause a gradual lowering of the fault resistance and an increase in fault current. We have observed this growth of the fault current during the first few cycles of the fault in our tests. In fact Mr. Jeerings observed this effect some years ago at R. G. & E. using a light beam oscillograph with 1200 Hz galvanometers.

We gather from Fig. 10, and other statements in the paper that all references to an arc are to the conditions within the soil and not to a visible arc in air between the conductor and the soil. The voltage breakdown phenomena within the soil is more complex than just an arc. In addition to thermal effects, there is also a voltage limiting action within the soil in the vicinity of the electrode similar to that of silicon carbide (thyrite). In view of this difference in action in air and in the soil, the industry needs a term other than arc to describe this complex action within the soil, such as, "Tharc" (short for thyrite + thermal + arc).

The ground fault laboratory simulation, Fig.5, illustrates the general nature of a HIGF, but it is not a true model of an actual fault condition. In an actual fault, all of the ground resistance is associated with the electrode/soil interface phenomena. There is no "ground return" resistance as shown in Fig. 5, since this is negligible, according to Kimbark [2]. The voltage gradients developed in Fig. 5, will not fully duplicate those in a HIGF and thus the resulting nonlinearities may not result in accurate harmonic data. How deep was the electrode inserted into the sand and was any attempt made to vary the fault current by this means?

Regarding the field test setup, why was a loop of wire used for the electrode rather than a straight length? Also, it is not clear how a steady fault current was limited to these low values. Can the authors give more detail on the test set up and especially on how a sustained fault current of less than five amperes was attained?

A HIGF instrument at the substation would need to separate the fault signals as shown in Fig.2, from the ambient shown in Fig. 3. Since these two signals are of comparable magnitude, would not a fault recognition relay need to respond to more than the magnitude of the harmonic currents?

A recent paper [3] by Kwon et al, on HIGF detection using even ordered harmonics, concluded that there is more randomness in the even ordered harmonics due to a fault than due to loads and he used this difference as a relay design parameter. Kwon was measuring phase currents as well as the neutral current.

References: [1] D. I. Jeerings, J. R. Linders, "Ground Resistance - Revisited", IEEE Transactions on Power Delivery, Vol. 4, No. 2, April 1989, pp949-956.

[2] E. W. Kimbark, "Dirct Current Transmission", (Book) John Wiley & Sons, New York, 1971 pp450-455.

[3] W. H. Kwon, Y. M. Park, G. W. Lee, "Detection of High Impedance Faults Using the Randomness of Even Harmonic Currents." IFAC International Symposium on Power Systems and Power Plant Control, Seoul, Korea, 1988, Paper No. M-11.

Manuscript received July 31, 1989.

A.E. Emanuel, D. Cyganski, J.A. Orr, S. Shiller and E.M. Gulachenski: The authors would like to thank Messrs Jeerings and Linders for their interest in the paper and the insightful questions. It is gratifying to realize that our effort helped to add a "quantum of new information to the arcing phenomenon in sandy soil". The comment made by our discussors regarding Fig. 10 prompted us to start a series of laboratory measurements under carefully controlled conditions. From these experiments we learned that fulgurites created in sandy soils act like linear resistors with a per unit length resistance of 2 to 100 $k\Omega/m$, high value for currents $< 0.5A$, low value for currents $> 3A$. The nonlinearity of the v/i is caused only by the arcing at the ends of the fulgurite. Sometimes a space between the conductor and the originating spot of the fulgurite will enable arcing to take place at the conductor surface. No "Tharc" phenomenon was observed in the sandy soils studied at WPI. Figure A confirms our claim. It represents the v/i characteristic of a prismatic body of sandy soil, $9 \times 6 \times 1.5cm$ with 10% initial moisture per volume. The voltage was applied at the $6 \times 1.5cm$ surfaces. The initial moisture delays the formation of arcing, and until the bulk of water is evaporated the studied sample acts as a linear resistor with $R \simeq 600\Omega$. When a separating wall of dry soil is formed arcing will start at the point of higher field intensity in the dry soil and the fulgurite starts to grow. During this interval the v/i characteristic is nonlinear. When the fulgurite bridges the electrodes and thermal equilibrium is attained a perfectly linear resistance with $R \simeq 5000\Omega$ was measured. Based on these type of experiments we conclude that the v/i characteristic stems only from the arcing phenomena at the leading ends of the fulgurite as well as at the originating spot of the fulgurite if the local geometry is such that a small air-gap was formed between the conductor and the fulgurite.

In the reference [2], Dr. Kimbark deals with the design of land electrodes. Such electrodes are meant to operate cold (at temperatures well below 100°C) and arcing must be totally avoided. When a conductor lies on the soil, fulgurites will form (due to arcing) and the fulgurites act like large resistors; therefore the "R, L arc" model is justified. The drawbacks of the experimental test described in Fig. 5 are the local electric field distribution, different than the real life case where the semi-infinite model applies, and the fact that the short circuit impedance of the system was larger than in typical situations. Our interest in small fault currents justified the insertion of additional series impedance. We did not attempt to vary the current by adjusting the depth of the insertion. The conductor was allowed to barely touch the soil surface. Our goal was to observe one point of contact only.

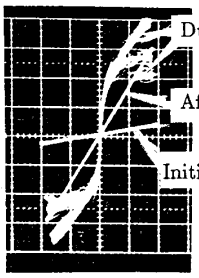

Fig. A Voltage-Current Characteristic of Sandy Soil in Nearly Uniform Electric Field. Vertical 1000 V/div, Horizontal 0.33 A/div

Fault currents are functions of soil resistivity, distance from the dropped conductor to the nearest ground electrode(s) connected to the neutral conductor, and the number of electrical points of contact between the dropped conductor and the soil. A straight conductor usually has one end touching the soil. Field stress amplification at the end favors the formation of arcing at the conductor's end. A loop can be viewed as an endless conductor, therefore giving more consistent performance. By varying the distance between the loop and a ground electrode it was possible to vary the fault current within large limits.

The answer to the last question regarding design of an arc fault relay is that this paper is not meant to provide a solution for a HIGF detector. It is a report based on experimental observations which we deemed worth sharing with the engineering community.

Manuscript received August 28, 1989.